

Fast extraction of resonant vibrational response from CARS spectra with arbitrary nonresonant background[†]

Yuexin Liu, Young Jong Lee, and Marcus T. Cicerone*

We describe a new, robust method of numerically extracting equivalent Raman spectra from coherent anti-Stokes Raman scattering (CARS) spectra. The extraction procedure requires no *a priori* information regarding the vibrational resonances or the shape of the nonresonant background (NRB). The method we present here is robust to situations where the NRB is not spectrally flat, and is accurate over a wide range of signal-to-background ratios. This simple and quick computation method, which relies primarily on a small number of fast Fourier transforms, could reasonably be used in conjunction with spectral imaging, where millions of spectra must be analyzed. Published 2009 by John Wiley & Sons, Ltd.

Keywords: spectroscopy; CARS; phase retrieval; Raman spectrum; nonresonant background

Introduction

Coherent anti-Stokes Raman scattering (CARS) microscopy provides excellent sensitivity, high spatial resolution and inherent chemical specificity, enabling the characterization of chemical species or biological components noninvasively, within complex heterogeneous systems in material science^[1,2] and biology.^[3] Due to the coherent addition of both resonant and nonresonant background (NRB) contributions, vibrational resonances in CARS spectra show apparent frequency shifts and differences in relative peak amplitude compared to the spontaneous Raman spectra.^[4] Details of the peak changes depend on resonant contributions from nearby peaks and the amplitude of the nonresonant contribution. Thus, the direct CARS intensity as such is not a good candidate for extracting quantitative composition information from a spectrum; the underlying Raman susceptibility is the more appropriate quantity for this purpose. The Raman response can be extracted by experimentally measuring both the real and imaginary part of the CARS spectrum.^[5,6] However, such methods introduce added complexity in the measurement apparatus, typically requiring careful control over the phase of the laser pulses employed in the experiments.^[7]

Besides these experimental methods, several numerical approaches^[4,7–9] have been employed to extract the equivalent Raman spectra from measured CARS spectra. The maximum entropy (ME) method calculates model parameters by solving a system of N coupled linear equations, with N being as large as half of the number of points in the spectrum.^[7,9,10] This system of coupled linear equations is a so-called Toeplitz system, and can be solved with specialized and efficient algorithms. In practice, a spectrum of interest is first normalized by a reference (NRB) spectrum. If the background amplitude varies with wavenumber, the phase is extracted with the assumption that the resonant structures are much smaller than the background at a given point in the CARS spectrum.^[7] For spectrally flat background, this assumption is not needed. The MEM approach has shown to be very reliable for quantitative retrieval of Raman spectra.^[7]

Recently, an adaptation of Fourier transform spectral interferometry (FTSI),^[11] has been demonstrated for extracting the resonant spectrum from a multiplex or broadband CARS signal.^[8] Using this method, the CARS spectrum is first normalized by a simultaneously measured nonresonant spectrum. The Raman spectrum is then extracted utilizing principles associated with the causality of the coherent vibration. However, as we will discuss below, normalization of the spectrum as by Lim *et al.*^[8] can adversely impact the shape and relative peak intensity of the retrieved Raman spectrum when the NRB is not spectrally flat. In the present study, we describe an alternative approach to numerically extract the Raman spectrum, the validity of which is not affected by the shape of the NRB. Similar to Refs [8 and 11], the principle of causality is applied to extract Raman lineshapes from CARS spectra, but the initial spectral normalization and concomitant sensitivity to the shape of NRB is avoided. The present method represents a further improvement in accuracy; we show that iterative consideration of higher terms in a Taylor series description of the signal, based on the residual between the original and extracted CARS spectra, can be used to correct spectral aberrations induced by approximations in the approach. This allows us to relax the condition that the nonresonant signal be much larger than the resonant one, making the spectral extraction more widely applicable. Because most operations used in the analysis are performed in the form of fast Fourier transform (FFT) and a single iteration of the process requires only two transforms be calculated, the computational demands of this method are relatively small.

* Correspondence to: Marcus T. Cicerone, Polymers Division, National Institute of Standards and Technology, Gaithersburg, MD 20899, USA.
E-mail: cicerone@nist.gov

[†] This work is a product of the U.S. Government and is not subject to copyright in the United States.

Polymers Division, National Institute of Standards and Technology, Gaithersburg, MD 20899, USA

Method

The CARS nonlinear susceptibility is given by^[8]

$$\begin{aligned} |\chi_{\text{CARS}}(\omega)|^{1/2} &\propto |\chi_{\text{CARS}}(\omega)| \\ &= [|\chi_{\text{NR}}(\omega)|^2 + |\chi_{\text{R}}(\omega)|^2 + 2\chi_{\text{NR}}(\omega)\text{Re}[\chi_{\text{R}}(\omega)]]^{1/2} \\ &= |\chi_{\text{NR}}(\omega)| [1 + |\chi_{\text{R}}(\omega)|^2/|\chi_{\text{NR}}(\omega)|^2 \\ &\quad + 2\text{Re}[\chi_{\text{R}}(\omega)]/|\chi_{\text{NR}}(\omega)|]^{1/2} \end{aligned} \quad (1)$$

The nonresonant signal, $\chi_{\text{NR}}(\omega)$, arising from the instantaneous electronic contributions, is purely real and frequency independent. A Taylor series expansion of the right-hand side of Eqn (1) yields,

$$\begin{aligned} |\chi_{\text{CARS}}| &= |\chi_{\text{NR}}| \times \{1 + \text{Re}[\chi_{\text{R}}]/|\chi_{\text{NR}}| - \text{Re}[\chi_{\text{R}}]^2/2| \\ &\quad \chi_{\text{NR}}|^2 + |\chi_{\text{R}}|^2/2|\chi_{\text{NR}}|^2 + \mathcal{O}[\chi_{\text{R}}^3] + \dots\} \end{aligned} \quad (2)$$

The terms in Eqn (2) are arranged according to powers of $\chi_{\text{R}}(\omega)$. When ignoring the terms containing powers of χ_{R} higher than one, we obtain an approximation for the CARS signal, involving the sum of the nonresonant signal and the real part of the resonant signal.

$$|\chi_{\text{CARS}}(\omega)| \approx |\chi_{\text{NR}}(\omega)| + \text{Re}[\chi_{\text{R}}(\omega)] \quad (3)$$

Note that the nonresonant component in CARS signal, $|\chi_{\text{NR}}(\omega)|$, is typically a smooth function in frequency; the sharp spectral features generally come from the resonant component. Equation (3) illustrates that, we can extract the Raman spectrum directly from CARS spectrum with no prior knowledge of the resonant spectrum itself, provided we have a reasonable guess for the nonresonant component. The nonresonant signal can be obtained either via experimental measurement of a reference sample under the same conditions or via numerical estimation from the CARS spectrum, such as a low-pass Fourier filtering.

Subtraction of the nonresonant signal from Eqn (3) allows us to retrieve the interferometric term $\text{Re}[\chi_{\text{R}}(\omega)]$ numerically,

$$|\chi_{\text{CARS}}(\omega)| - |\chi_{\text{NR}}(\omega)| \approx \text{Re}[\chi_{\text{R}}(\omega)] \quad (4)$$

The resonant signal, $\chi_{\text{R}}(\omega)$, is a complex quantity, with a real and an imaginary part. Because the resonant signal is generated by the Raman response of the sample, the inverse Fourier transform of the resonant susceptibility $\chi_{\text{R}}(\omega)$ is the Raman response function of the sample in the time domain, $h_{\text{R}}(t)$. The inverse Fourier transform of $\text{Re}[\chi_{\text{R}}(\omega)]$ gives a related function:

$$\mathfrak{S}^{-1}\{\text{Re}[\chi_{\text{R}}(\omega)]\} = \left[\frac{h_{\text{R}}(t) + h_{\text{R}}^*(-t)}{2} \right] \quad (5)$$

where \mathfrak{S}^{-1} denotes the inverse Fourier transform. Thus, an approximation to $h_{\text{R}}(t)$ can be extracted simply by applying the Heaviside function, $u(t) = \begin{cases} 1, & t \geq 0 \\ 0, & t < 0 \end{cases}$, to the inverse Fourier transform of the left hand side of Eqn (4):

$$\begin{aligned} u(t) \times \mathfrak{S}^{-1}[|\chi_{\text{CARS}}(\omega)| - |\chi_{\text{NR}}(\omega)|] &\approx u(t) \\ &\times \left[\frac{h_{\text{R}}(t) + h_{\text{R}}^*(-t)}{2} \right] = \frac{h_{\text{R}}(t)}{2} \end{aligned} \quad (6)$$

The physical justification for application of $u(t)$ is that the time evolution of the coherent vibration should have a zero amplitude

before the molecular excitation takes place.^[8,12,13] The complex quantity of the resonant CARS spectrum in the frequency domain is obtained via Fourier transform of Eqn (6).

$$\begin{aligned} \mathfrak{S}\{u(t) \times \mathfrak{S}^{-1}[|\chi_{\text{CARS}}(\omega)| - |\chi_{\text{NR}}(\omega)|]\} \\ \approx \mathfrak{S}\left[\frac{h_{\text{R}}(t)}{2}\right] = \frac{\chi_{\text{R}}(\omega)}{2} \end{aligned} \quad (7)$$

The imaginary part of Eqn (7), thus gives the approximate Raman spectrum corresponding to the CARS spectrum.

The current method is different from the previously reported half-sided Fourier method^[8] in that here we subtract the estimated NRB term rather than use it to normalize the spectrum, and we use successive approximations to converge on to a faithful representation of the resonant signal. For the method presented in Ref. [8], the interferometric term $\text{Re}[\chi_{\text{R}}(\omega)]$ is multiplied by the nonresonant signal. This was justified on the basis that the nonresonant signal is smooth, and it was implied that the procedure should not impact the retrieved spectrum too much. However, based on the convolution theorem, a multiplication in the time domain is equal to a convolution in the frequency domain, and thus, using this approach, the Fourier transform of the nonresonant signal is convolved with the Fourier transform of the interferometric term. An NRB signal that is not flat will have a Fourier transform (time representation) that is not a delta function and will modify the line shapes of the extracted Raman spectrum in terms of transition frequency, line width and peak intensity. This situation becomes even worse if the nonresonant signal $|\chi_{\text{NR}}|$ in the CARS signal has a slightly different shape from the separately measured reference signal $|\chi_{\text{ref}}|$. Thus, the prefactor term $|\chi_{\text{NR}}|/|\chi_{\text{ref}}|^{[2]}$ in Ref. [8] that resulted from normalization may not be a smooth function even though both $|\chi_{\text{NR}}|$ and $|\chi_{\text{ref}}|$ are smooth functions. In contrast, in the present method we obtain the interferometric term with the nonresonant signal added rather than multiplied (Eqn (3)). Since the Fourier transformations are linear operations, the nonresonant signal in this equation only gives the background level, but does not change the lineshapes of the extracted Raman spectrum.

Results and Discussion

Figure 1 displays output from the method described above; the inset shows a simulated CARS spectrum, which is obtained via a coherent summation of several Lorentzian lineshape functions and a background. Note that the non-resonant signal is not flat but is a smooth function of frequency; the present extraction method can accommodate NRB of essentially any shape. We obtain an approximation to $\text{Re}[\chi_{\text{R}}]$ according to Eqn (4) by subtracting the nonresonant signal from the raw CARS signal. We then extract the equivalent resonant spectrum (i.e. the Raman spectrum) following the algorithm described above, embodied in Eqn (7). The extracted Raman spectrum (dotted line) is plotted, along with the simulated spectrum (solid line) in the main portion of Fig. 1. In spectral regions where all the resonant peak intensities are small we see good agreement between the extracted and simulated (reference) spectra. Larger deviations are observed when the Raman peak intensities are higher, as is expected from the approximation in Eqn (3). Figure 1 also displays a Raman spectrum extracted using the approach of Ref. [8], after scaling by the original NRB in order to more closely match the reference spectrum (dashed line). Using that approach, the deviations in the larger intensities Raman peaks

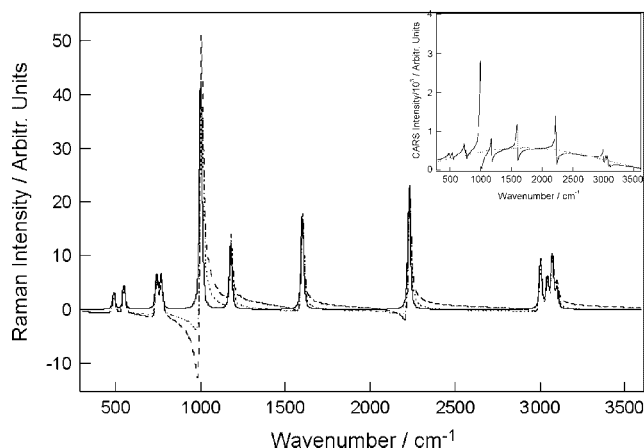


Figure 1. Simulated Raman spectrum (solid), extracted Raman spectrum (dotted) using the approach of this paper, and extracted Raman spectrum (dashed) using the approach of Ref. [8] where the spectrum is scaled by the nonresonant signal. Inset: simulated CARS (solid) and nonresonant reference (dotted) spectra.

are exaggerated as compared to those obtained by the present approach. Differences in peak shape between these two extracted spectra are due to artifacts introduced in Ref. [8] by normalizing the CARS spectrum to a non-flat NRB.

For the larger peaks in Fig. 1, the primary source of deviation between the reference spectrum and spectrum retrieved by the present approach arises from the implicit assumption that $|\chi_R(\omega)|/|\chi_{NR}(\omega)|$ is small when higher order terms are ignored in Eqn (3). Provided this ratio is not too large (see below), the errors that arise from this assumption can be rectified in an iterative fashion. This is done by first back-calculating a CARS spectrum using the *extracted* $\chi_R(\omega)$ term (dotted curve in Fig. 1) and the $\chi_{NR}(\omega)$ term. The difference, or residual, between this back-calculated spectrum and the observed CARS spectrum is then calculated. An approximate expression describing this residual function is obtained by including the terms quadratic in $\chi_R(\omega)$ from Eqn (2) as follows:

$$\chi_{res} = |\chi_{orig}| - |\chi_{extr}| \approx |\chi_{NR}| \times \left\{ -\frac{\text{Re}[\chi_R]^2}{2|\chi_{NR}|^2} + \frac{|\chi_R|^2}{2|\chi_{NR}|^2} \right\} \quad (8)$$

where the subscripts res, orig, and extr denote residual, original and extracted. Note that $\text{Im}[\chi_{orig}]$ is that we ultimately wish to extract, and this is accomplished when $\chi_{res} = 0$.

Because the nonresonant response functions used in the original and extracted CARS spectra are identical, they cancel when the inverse Fourier transform of Eqn (8) is taken. Thus, the positive-time half of the inverse Fourier transform of χ_{res} gives the approximate difference between the original and extracted Raman responses in the time domain.

$$u(t) \times \mathfrak{S}^{-1}[\chi_{res}] \approx \frac{h_{R,orig}(t) - h_{R,extr}(t)}{2} \quad (9)$$

In a similar manner, the Fourier transform of Eqn (9) yields the difference between the original and extracted Raman spectra in the frequency domain.

$$\mathfrak{S}\{u(t) \times \mathfrak{S}^{-1}[\chi_{res}]\} \approx \frac{\chi_{R,orig}(\omega) - \chi_{R,extr}(\omega)}{2} \quad (10)$$

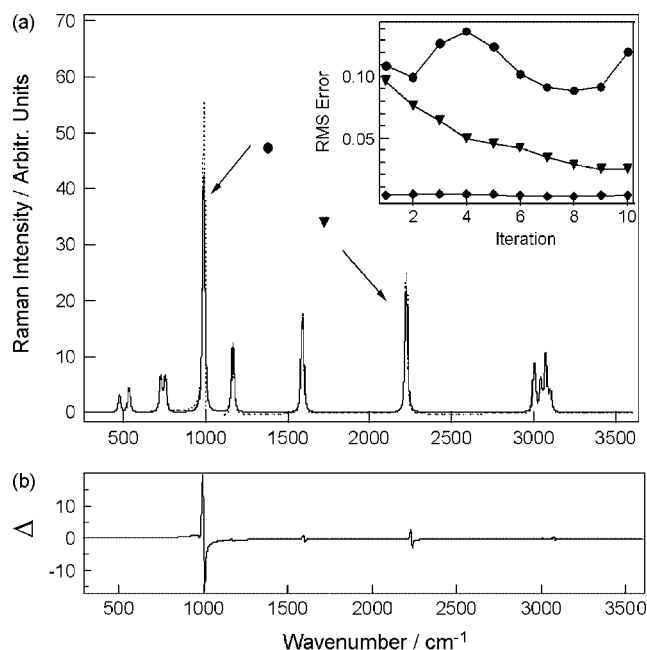


Figure 2. (a) Improved Raman spectrum (dotted) after 10 iterations of the process described by Eqns (8)–(11) (see text) as compared to the simulated Raman spectrum (solid) from Fig. 1. Inset: RMS deviations of extracted spectrum from simulated spectrum, as a function of number of iterations of the process described by Eqns (8)–(11). (▼) in the vicinity of 2250 cm^{-1} peak, (●) vicinity of the 1000 cm^{-1} peak and (◆) the remainder of the extracted spectrum. (b) Difference between the reference spectrum and the extracted Raman spectrum shown in (a).

From Eqn (10), we obtain the next approximation to the original Raman lineshapes as follows:

$$\text{Im}\{\chi_{R,orig}\} \approx \text{Im}\{\chi'_{extr}\} = \text{Im}\{\chi_{extr}\} + \text{Im}\{2 \times \mathfrak{S}\{u(t) \times \mathfrak{S}^{-1}[\chi_{res}]\}\} \quad (11)$$

The second term in the right-hand side of Eqn (11) is the correction term based on the spectral residual.

The iterative process, analogous to Eqns (8)–(11) can be repeated as many times as necessary, using increasingly larger powers of χ_R . The main panel of Fig. 2(a) shows the simulated Raman spectrum from Fig. 1, and the Raman spectrum extracted after a single iteration of the process described by Eqns (8)–(11). The difference between the reference Raman spectrum and the extracted Raman spectrum, $(\text{Im}[\chi'_{extr}])$ is plotted in the lower panel of Fig. 2(b). The differences are negligible for all isolated peaks and congested clusters of peaks in the spectrum where $|\chi_R(\omega)|/|\chi_{NR}(\omega)| \leq 1$, but there are significant differences for the larger peaks. An indication of improvements to fit with further iterations, using higher order terms in the Taylor series, is plotted in the inset to Fig. 2(a). Triangles in this plot indicate the absolute RMS deviations in the vicinity of the 2250 cm^{-1} peak, where the ratio $|\chi_R(\omega)|/|\chi_{NR}(\omega)|$ is approximately 2; deviations decrease monotonically with implementation of finer approximations in the Taylor series, up to 10 iterations. The circles indicate RMS deviations in the vicinity of the 1000 cm^{-1} peak, where $|\chi_R(\omega)|/|\chi_{NR}(\omega)| \approx 4$. Here, deviations simply oscillate with iteration number, showing no clear sign of convergence. The remainder of the extracted spectrum conforms to the original spectrum very well, with absolute RMS errors of approximately 0.003, and no substantial changes after the first iteration.

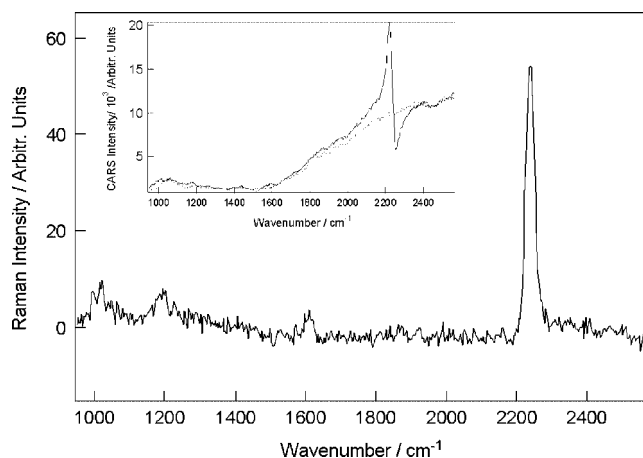


Figure 3. Extracted Raman spectrum of benzonitrile in ethanol at a concentration of 1 mol/L. Spectrum was extracted using Eqn (7), with no further iterations. Inset: the experimental CARS spectrum (solid) and separately measured nonresonant background (dotted). Standard uncertainty of wavenumber was $\pm 3 \text{ cm}^{-1}$.

Experimental verification of the signal extraction approach is demonstrated in Fig. 3; the inset shows an experimental CARS spectrum of benzonitrile in ethanol at a concentration of 1 mol/L, with a separately measured NRB. The CARS intensity is very low at wavenumber $< 1700 \text{ cm}^{-1}$ due to a supercontinuum pulse that was weak in that spectral region. The experimental spectra presented in this paper are acquired by using the setup described in the Ref. [5]. The main part of Fig. 3 shows the Raman spectrum retrieved from the data in the inset, using the procedure described in Eqn (7), with no further iterations. Note that all peaks in the vicinity of $(1000, 1180 \text{ and } 1600) \text{ cm}^{-1}$ are faithfully retrieved, even though their presence is not obvious in the original data. Thus, we demonstrate that this approach can be used to rapidly retrieve even very weak resonant vibrational signals from a CARS spectrum when the NRB has been measured separately.

As is the case for the data in Fig. 3, the nonresonant signal is often obtained by measuring a reference sample under the same conditions as used to obtain the feature CARS spectrum. However, one can imagine scenarios, wherein the nonresonant susceptibility of the sample of interest could be slightly different from that of a reference sample. For example, a nearby 2- or 3-photon resonance in a protein backbone may slightly alter the shape of the nonresonant susceptibility compared to that of a reference obtained from a coverslip. This is a particular concern when a broad vibrational spectrum is being collected. To avoid this possibility, the reference NRB is often collected in the sample itself,^[5,8] even though this will lead to increased photodamage for delicate samples. In the interest of improved signal throughput and reduced potential for photodamage, it may be beneficial in some cases to be able to reliably extract the resonant signal having only approximate knowledge of the NRB spectral shape, or having no prior knowledge at all. Below we describe an approach to an ‘unsupervised’ (automated) estimation of the NRB and subsequent extraction of the Raman-like resonant component from a CARS spectrum. The approach described below takes advantage of the spectral extraction method described above; it is made feasible by the meager computational demands and the rapidity with which the method described in Eqns (7)–(11) we can arrive at a reasonable approximation to the resonant spectrum.

If no specific prior knowledge of the NRB exists, a first estimation of the NRB can be obtained from information contained in the short-time component of the time-domain representation of the CARS spectrum, since this is dominated by the nonresonant response. Naturally, such a filtering approach requires one to set a spectral feature ‘sharpness’ criterion – sharper features would be considered as resonant, and broader features would be accounted for as NRB. Just how to set such a criterion would depend on the general shapes of the NRB and the spectral features of interest. Setting such a criterion would be relatively straightforward in most cases, with the possible exception of very broad features, such as the OH stretch in water, or of rapidly varying NRB amplitudes. The specific details of the filter used to obtain the ‘short time’ component are not very important in this context, since errors in the first estimation will be corrected.

Recognizing the fact that we don’t have the correct shape of the NRB, we modify Eqn (4) as follows:

$$|\chi_{\text{CARS}}(\omega) - |\chi'_{\text{NR}}(\omega)| \approx (|\chi_{\text{NR}}(\omega)| - |\chi'_{\text{NR}}(\omega)|) + \text{Re}[\chi_{\text{R}}(\omega)] \quad (12)$$

where $|\chi'_{\text{NR}}(\omega)|$ is the first estimate of the nonresonant signal, either from experimental measurement or numerical estimation from the raw CARS spectrum, and $|\chi_{\text{NR}}(\omega)|$ is the actual nonresonant signal. We then apply the approach described by Eqn (7) to obtain:

$$\text{Im}\{\text{HSF}[|\chi_{\text{CARS}}(\omega) - |\chi'_{\text{NR}}(\omega)|]\} \approx \text{Im}\{\text{HSF}[\text{Re}[\chi_{\text{R}}(\omega)]]\} + \text{Im}\{\text{HSF}[|\chi_{\text{NR}}(\omega) - |\chi'_{\text{NR}}(\omega)|]\} \quad (13)$$

where $\text{HSF}[\chi(\omega)] = u(t) \times \mathfrak{I}^{-1}[\chi(\omega)]$.

The second term on the right-hand side of Eqn (13) is an error term which appears as a baseline offset to the signal of interest, and is nonzero when the actual and estimated nonresonant signals are not identical. In general, a Raman spectrum extracted using an approximate NRB shape and the approach described in Eqns (7)–(11) will have a nonzero baseline offset corresponding to the function $\text{Im}\{\text{HSF}[|\chi_{\text{NR}}(\omega) - |\chi'_{\text{NR}}(\omega)|]\}$, irrespective of the number of iterations. Thus, the problem of extracting the signal with no prior knowledge of the resonant or nonresonant parts is transformed to the simpler problem of determining the baseline offset of an extracted Raman spectrum.

In order to differentiate between the Raman signal and the baseline offset, we make a single, simple assumption regarding the NRB, that it has a given degree of spectral ‘smoothness’. In other words, that it is not responsible for sharp features of the extracted Raman spectrum. This assumption may not always be valid for 2-color CARS spectra generated using supercontinuum, but it is the most minimal constraint we can apply, and works remarkably well. We implement a procedure to discriminate between Raman spectral features and the baseline offset based on the smoothness ansatz by determining the local slope at each spectral data point (sampled over three neighboring data points). Those data points with a local slope that is sufficiently small are designated as baseline data. This process generates short segments of contiguous baseline data points, interrupted by gaps at locations of Raman peaks. We then assign knot points at a fixed interval (e.g. 30 cm^{-1}) along the baseline segments and at their endpoints, and generate a cubic spline to approximate our baseline correction function $\text{Im}\{\text{HSF}[|\chi_{\text{NR}}(\omega) - |\chi'_{\text{NR}}(\omega)|]\}$. The ‘stiffness’ of the correction function that we specify is determined by the maximum local slope allowed in determining the set of baseline points, and by the spacing of the knot points.

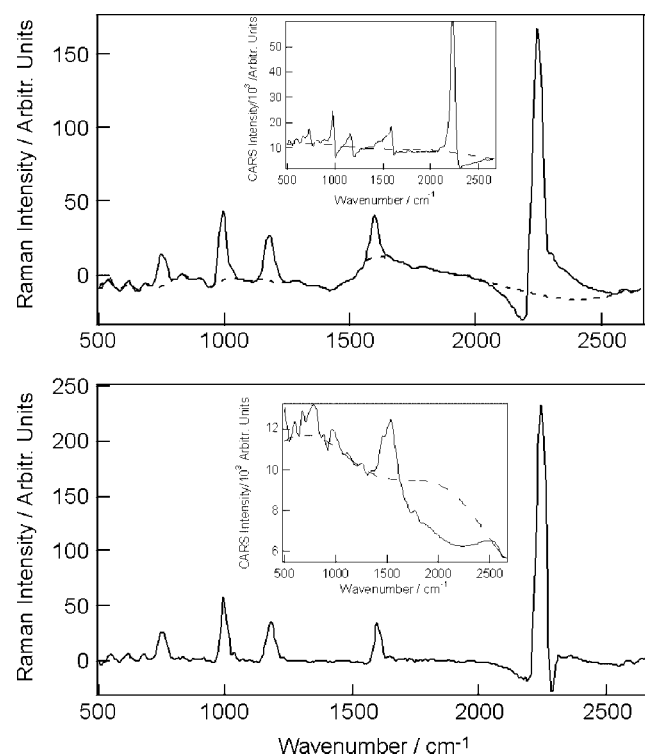


Figure 4. (a) Extracted Raman spectrum (solid) using the first estimate of NRB with four iterations, and the interpolated baseline (dotted) using the knot and spline procedure (see text) where the maximum slope was set to 0.24 cm^{-1} , and the knot interval was 31 cm^{-1} . Inset: the experimental CARS spectrum of pure benzonitrile (solid) and the first estimate of the nonresonant signal (dotted) generated from the short-time components of the time-domain CARS response. (b) Improved Raman spectrum using the corrected estimate of NRB with four iterations. The corrected estimate of NRB is obtained based on the first estimation and the interpolated baseline in (a). (see text) Inset: corrected estimate of NRB (solid) as compared to the original estimate of NRB (dotted). Standard uncertainty of wavenumber was $\pm 3 \text{ cm}^{-1}$.

Once baseline, i.e. the imaginary component of the function $\text{HSF}[|\chi_{\text{NR}}(\omega)| - |\chi'_{\text{NR}}(\omega)|]$ is determined, we can use the half-sided Fourier transform and the principle of causality to determine its companion real component. We add this real portion to our original estimate of the NRB to obtain a corrected NRB, and with that we repeat the procedure outlined in Eqns (7)–(11) to extract a corrected Raman signal.

Figure 4 illustrates the implementation of this procedure. The inset of Fig. 4(a) shows an experimental CARS spectrum of benzonitrile, and an estimation of the nonresonant signal generated from the short-time component of the time-domain CARS response. The main part of Fig. 4(a) shows the Raman spectrum extracted using the estimated NRB with four iterations of the extraction procedure described in Eqns (7)–(11). There are clear artifacts in the vicinity of the 2230 cm^{-1} peak; they are due to the high signal/NRB ratio in this peak, and do not diminish with corrective iterations, up to 10 iterations, similar to behavior seen in the 1000 cm^{-1} peak of Fig. 1. The estimation of $\text{Im}\{\text{HSF}[|\chi_{\text{NR}}(\omega)| - |\chi'_{\text{NR}}(\omega)|]\}$ is also plotted, as determined by the knot and spline procedure described above. The maximum slope was set to 0.24 cm^{-1} , and the knot interval was 31 cm^{-1} in this case. The interpolated baseline follows the baseline of the Raman spectrum quite well, except in the vicinity of the 2230 cm^{-1} peak, where we allow deviation in the presence of a known artifact.

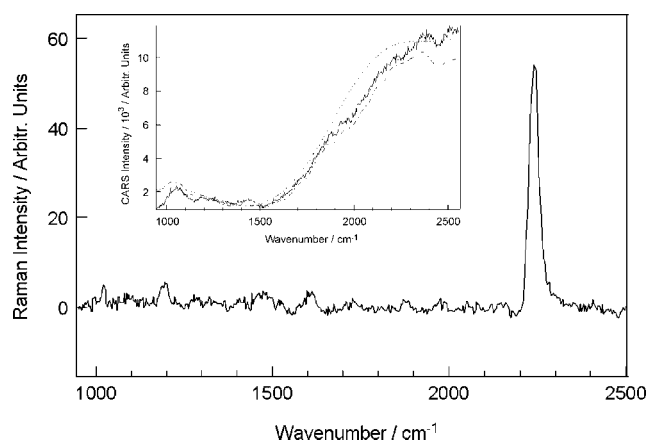


Figure 5. Raman spectrum extracted from the CARS data of Fig. 3, but using only an estimate of the NRB. The maximum accepted slope was set to 0.16 cm^{-1} , and the knot interval was 32 cm^{-1} for the baseline interpolation in this case. Inset: comparison of the experimental measured (solid), the first estimated (dotted), and the corrected (dashed) NRBs. Standard uncertainty of wavenumber was $\pm 3 \text{ cm}^{-1}$.

The inset to Fig. 4(a) shows the CARS spectrum and the original estimate of the NRB, used to extract the Raman spectrum plotted in the main portion of the figure. The inset to Fig. 4(b) shows the original approximation to the NRB, as plotted in the inset to Fig. 4(a). Also plotted is the corrected NRB estimate, which is used along with the original CARS spectrum to calculate the extracted Raman spectrum in the main part of Fig. 4(b).

Figure 5 shows a Raman spectrum extracted from the data of Fig. 3, but using an NRB function estimated as in Fig. 4(b) rather than the experimentally measured NRB. The fact that we recover all of the peaks is remarkable, given the low signal-to-noise ratio for the peaks in the region $1000\text{--}1700 \text{ cm}^{-1}$. The intensity of those low-energy peaks is slightly reduced compared to that shown in Fig. 3 where the measured NRB function was used in the extraction process. This slight reduction in amplitude is an artifact of the baseline fitting procedure; a slightly stiffer baseline fit would yield higher peaks in this region, but would also potentially introduce more spurious features such as the broad feature at approximately 1500 cm^{-1} . We note that this sensitivity of peak height to the stiffness of the baseline fit is significant only for very small peaks. The small contributions to peak height with stiffer fitting are insignificant for large peaks such as the 2230 cm^{-1} peak in this figure. The inset to Fig. 5 shows the NRB functions associated with the data in the main plot. Included are the first estimate and the corrected estimate of the NRB; the measured NRB is also included for reference, although it was not used in generating the extracted Raman spectrum. The corrected estimate of the NRB has a spectral shape that is very close to the measured NRB, and this is consistent with the faithfully extracted Raman signal.

Naturally, the ‘smoothness’ ansatz we employ in estimating the NRB should work best for cases where the nonresonant background is spectrally smooth. Most of the methods used for generating multiplex and broadband CARS signals, do in fact, yield spectrally smooth NRB, including 3-color CARS schemes^[8,14,15] where any irregularities in spectral envelope are smoothed out by convolution inherent in intrapulse excitation, and 2-color CARS schemes if both pulses are spectrally smooth.^[16] The most stringent challenge to the smoothness ansatz is likely to come from 2-color CARS generation when the Stokes pulse has sharp spectral features and oscillations as are often seen in pulses broadened in a

nonlinear fiber such as for the experimental data in this paper. The shape of the NRB is a direct convolution of the spectral shapes of the pump-probe and the Stokes pulses in a 2-color CARS spectrum.

Conclusion

In conclusion, we have described a new, rapid, and computationally simple approach for numerically extracting an equivalent Raman spectrum from a CARS spectrum that is valid with arbitrarily-shaped NRB and resonant/nonresonant signal ratios up to at least 2. The method requires no specific *a priori* information regarding either the vibrational resonances or the NRB, and is applicable to isolated peaks, or to congested spectral regions. The fact that the computation involved in signal extraction is simple and rapid makes this a good candidate for use in imaging applications.

References

- [1] T. W. Kee, M. T. Cicerone, *Opt. Lett.* **2004**, *29*, 2701.
- [2] B. G. Saar, H. S. Park, X. S. Xie, O. D. Lavrentovich, *Opt. Lett.* **2007**, *15*, 13585.
- [3] C. L. Evans, X. S. Xie, *Annu. Rev. Anal. Chem.* **2008**, *1*, 883.
- [4] H. A. Rinia, M. Bonn, M. Muller, *J. Phys. Chem. B* **2006**, *110*, 4472.
- [5] T. W. Kee, H. X. Zhao, M. T. Cicerone, *Opt. Express* **2006**, *14*, 3631.
- [6] E. O. Potma, C. L. Evans, X. S. Xie, *Opt. Lett.* **2006**, *31*, 241.
- [7] E. M. Vartiainen, H. A. Rinia, M. Muller, M. Bonn, *Opt. Express* **2006**, *14*, 3622.
- [8] S. H. Lim, A. G. Caster, S. R. Leone, *Opt. Lett.* **2007**, *32*, 1332.
- [9] E. M. Vartiainen, *J. Opt. Soc. Am. B* **1992**, *9*, 1209.
- [10] G. I. Petrov, R. Arora, V. V. Yakovlev, X. Wang, A. V. Sokolov, M. O. Scully, *Proc. Natl. Acad. Sci. U.S.A.* **2007**, *104*, 7776.
- [11] L. Lepetit, G. Cheriaux, M. Joffre, *J. Opt. Soc. Am. B* **1995**, *12*, 2467.
- [12] E. M. Vartiainen, K. E. Peiponen, T. Asakura, *Appl. Spectrosc.* **1996**, *50*, 1283.
- [13] B. C. Chen, S. H. Lim, *J. Phys. Chem. B* **2008**, *112*, 3653.
- [14] Y. J. Lee, Y. X. Liu, M. T. Cicerone, *Opt. Lett.* **2007**, *32*, 3370.
- [15] D. Oron, N. Dudovich, D. Yelin, Y. Silberberg, *Phys. Rev. Lett.* **2002**, *88*, 063004.
- [16] M. Muller, J. M. Schins, *J. Phys. Chem. B* **2002**, *106*, 3715.